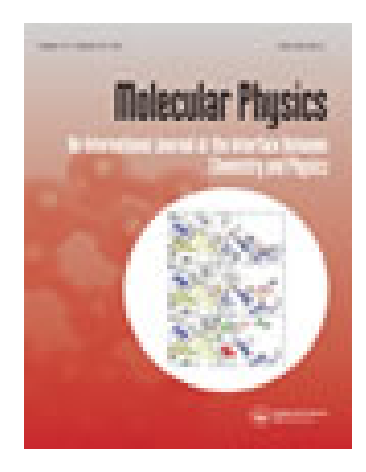
This article was downloaded by: [Washington University in St Louis]

On: 06 October 2014, At: 00:13 Publisher: Taylor & Francis

Informa Ltd Registered in England and Wales Registered Number: 1072954 Registered office: Mortimer House,

37-41 Mortimer Street, London W1T 3JH, UK



Molecular Physics: An International Journal at the Interface Between Chemistry and Physics

Publication details, including instructions for authors and subscription information: http://www.tandfonline.com/loi/tmph20

Combining spin-adapted open-shell TD-DFT with spin-orbit coupling

Zhendong Li ^a , Bingbing Suo ^a , Yong Zhang ^a , Yunlong Xiao ^a & Wenjian Liu ^a ^a Beijing National Laboratory for Molecular Sciences, Institute of Theoretical and Computational Chemistry, State Key Laboratory of Rare Earth Materials Chemistry and Applications, College of Chemistry and Molecular Engineering, and Center for Computational Science and Engineering , Peking University , Beijing , 100871 , People's Republic of China

Accepted author version posted online: 17 Apr 2013. Published online: 29 Nov 2013.

To cite this article: Zhendong Li, Bingbing Suo, Yong Zhang, Yunlong Xiao & Wenjian Liu (2013) Combining spin-adapted open-shell TD-DFT with spin-orbit coupling, Molecular Physics: An International Journal at the Interface Between Chemistry and Physics, 111:24, 3741-3755, DOI: 10.1080/00268976.2013.785611

To link to this article: http://dx.doi.org/10.1080/00268976.2013.785611

PLEASE SCROLL DOWN FOR ARTICLE

Taylor & Francis makes every effort to ensure the accuracy of all the information (the "Content") contained in the publications on our platform. However, Taylor & Francis, our agents, and our licensors make no representations or warranties whatsoever as to the accuracy, completeness, or suitability for any purpose of the Content. Any opinions and views expressed in this publication are the opinions and views of the authors, and are not the views of or endorsed by Taylor & Francis. The accuracy of the Content should not be relied upon and should be independently verified with primary sources of information. Taylor and Francis shall not be liable for any losses, actions, claims, proceedings, demands, costs, expenses, damages, and other liabilities whatsoever or howsoever caused arising directly or indirectly in connection with, in relation to or arising out of the use of the Content.

This article may be used for research, teaching, and private study purposes. Any substantial or systematic reproduction, redistribution, reselling, loan, sub-licensing, systematic supply, or distribution in any form to anyone is expressly forbidden. Terms & Conditions of access and use can be found at http://www.tandfonline.com/page/terms-and-conditions



RESEARCH ARTICLE

Combining spin-adapted open-shell TD-DFT with spin-orbit coupling

Zhendong Li, Bingbing Suo, Yong Zhang, Yunlong Xiao and Wenjian Liu*

Beijing National Laboratory for Molecular Sciences, Institute of Theoretical and Computational Chemistry, State Key Laboratory of Rare Earth Materials Chemistry and Applications, College of Chemistry and Molecular Engineering, and Center for Computational Science and Engineering, Peking University, Beijing 100871, People's Republic of China

(Received 20 January 2013; final version received 8 March 2013)

The recently proposed spin-adapted time-dependent density functional theory (S-TD-DFT) is extended to the relativistic domain for fine-structure splittings of excited states of open-shell systems. Scalar-relativistic effects are treated to infinite order via the spin-free (sf) part of the exact two-component (X2C) Hamiltonian, whereas the spin-orbit couplings (SOC) between the scalar-excited states are treated perturbatively via an effective one-electron spin-orbit operator derived from the same X2C Hamiltonian. The calculated results for prototypical open-shell systems containing heavy elements reveal that the composite approach sf-X2C-S-TD-DFT-SOC is very promising. The fine-structure splitting of a spatially degenerate ground state can also be described properly by taking a non-degenerate excited state as the reference.

Keywords: spin-adapted TD-DFT; spin-free X2C; spin-orbit coupling; fine structure; open-shell systems

1. Introduction

Excited states of open-shell molecular systems remain to be a great challenge to quantum chemistry. While multireference wave-function-based methods can usually 'get the right answer for the right reason', they are computationally too expensive and applicable only to small systems. In addition, the choice of active space and the corresponding multi-configuration self-consistent-field calculations are often not straightforward. This complexity is formally avoided by single-reference wave-function- or density-functional-based methods. Yet, such methods require in principle higher excitation ranks to achieve the same accuracy as multi-reference approaches. The symmetrisation of spin and spatial degrees of freedom, a highly non-trivial issue, must also be taken into account. Otherwise, the calculated results might be physically meaningless. Taking time-dependent density functional theory (TD-DFT) [1] as an example, a straight calculation in terms of unrestricted Kohn-Sham orbitals (U-TD-DFT) may produce states with substantial spin contamination [2]. A direct consequence is that the excitation energies of such states might significantly be underestimated, e.g. by approximately 2 eV or 20% for the $2^2\Sigma_{\mu}^+$ state of N_2^+ [3]. The mean absolute error (MAE) for the lowest eight excited states of N_2^+ obtained with the local density approximation (LDA) amounts to 0.88 eV [3], which is much larger than the typical errors (0.2–0.3 eV [4]) of TD-DFT for singlet excited states of well-behaved closed-shell systems. Such spin contamination stems from the fact that the underlying adiabatic approximation can access only single excitations whereas certain class of doubles and even higher excitations must be included to achieve spin adaptation. This apparent paradox is resolved only recently via the tensor-coupling scheme [5,6], which takes all the components of a multiplet of spin S_i as the reference and further allows spin-flip transitions in conjunction with the non-collinear exchangecorrelation (XC) kernel [7-10]. The excitation manifold, generated through only single excitations though, is spin complete and can be decomposed into a direct sum of subspaces of spin $S_i = S_i - 1$, S_i , and $S_i + 1$. By virtue of the Wigner-Eckart theorem, the final working equations of the so-obtained spin-adapted TD-DFT (S-TD-DFT) involve explicitly only the high-spin component of the reference multiplet S_i , such that the states of spin $S_i = S_i - 1$, S_i , and $S_i + S_i$ 1 can be obtained in one shot. As such, the spin adaptation of TD-DFT is indeed possible within the adiabatic approximation. As expected, S-TD-DFT improves greatly over U-TD-DFT for those heavily spin-contaminated states [6]. However, the accuracy of S-TD-DFT for high-spin openshell systems is still, in average, inferior to TD-DFT for well-behaved closed-shell systems. The primary reason can be traced back to the fact that approximate XC functionals do not fulfil the necessary conditions for ensuring the strict degeneracy of different components of an excited multiplet. Fortunately, this defect can nicely be corrected [3] by combining the good of S-TD-DFT and S-RPA (random phase approximation). The former yields a good estimate of the averaged energies of the multiplets whereas the latter gives

^{*}Corresponding author. Email: liuwj@pku.edu.cn

rise to a good estimate of their separations. Although such hybridisation is based solely on a formal basis, the resulting ansatz X-TD-DFT does further improve S-TD-DFT. For instance, the MAE for the lowest eight states of N₂⁺ is 0.39 eV by S-TD-DFT but becomes 0.24 eV by X-TD-DFT [3]. X-TD-DFT is also computationally cheaper than the parent S-TD-DFT. The implementation of X-TD-DFT is truly simple. Only a few Fortran lines of code need to be inserted into an existing U-TD-DFT module. The calculation then proceeds as U-TD-DFT but with restricted open-shell Kohn–Sham (ROKS) orbitals as input. Therefore, it is X-TD-DFT [3] that should be recommended for routine calculations of scalar states of open-shell systems.

Apart from the proper treatment of spin symmetry. another closely related issue is how to account for spinorbit couplings (SOC) within TD-DFT. This can, in principle, be done in two different ways, either jj or LS coupling. The former includes four-component (4C) and twocomponent (2C) relativistic TD-DFT. 4C-TD-DFT, along with a non-collinear XC kernel, was first developed by the present authors [8,9]. Note that the use of the noncollinear XC kernel is mandatory for properly describing the SOC even of closed-shell systems. It was then shown [10] that, when the time-reversal symmetry is properly handled, both 4C- and 2C-TD-DFT can, without much loss of accuracy (<0.001 eV), be reduced to the familiar form known from non-relativistic TD-DFT [11]. That is, the spin-dependent and spin-free versions of closed-shell TD-DFT can actually adopt the same matrix form. This unified formulation facilitates greatly the use of molecular symmetry of arbitrary orders [12]. A different implementation of 4C-TD-DFT was reported by Bast et al. [13] but following the same concept of the non-collinear XC kernel [7-10]. The implementations of 2C-TD-DFT differ mainly in the Hamiltonians, either exact [13–15] or approximate [10,16,17]. Not surprisingly, such relativistic TD-DFT for closed-shell systems containing heavy elements have similar accuracy as non-relativistic TD-DFT for closed-shell systems of light elements. As for openshell systems, straight 4C/2C-TD-DFT calculations will encounter 'moment contamination' (the relativistic analogue of spin contamination), even with Kramers-restricted Kohn-Sham spinors subject to both time-reversal and double group symmetries [12]. This is because the single excitation manifold from a single reference determinant is generally not invariant under the action of time-reversal or double group operations. The tensor-coupling scheme [5,6] for the spin adaptation of non-relativistic open-shell TD-DFT can, in principle, be employed here for the moment adaptation of 4C-/2C-TD-DFT, without going beyond the adiabatic approximation. However, this is only true if the reference state $|\Phi_0\rangle$ and its Kramers partner $|\bar{\Phi}_0\rangle = \mathcal{K}|\Phi_0\rangle$ can indeed form a tensor reference. That is, they must belong to different columns of the same irreducible representation (irrep) of a double point group, such that the use of the Wigner-Eckart theorem can be made. For atoms, this condition is naturally satisfied. Starting from a tensor reference $\{|j_0m_0\rangle, m_0 = -j_0, ..., j_0\}$, all the matrix elements of a relativistic Hamiltonian H between single excitations $a_{j_1m_2}^{\dagger}a_{j_1m_1}|j_0m_0\rangle$ can be assembled in terms of the matrix elements between single excitations from the high-moment component $|j_0j_0\rangle$ alone. For molecules, such a reduction is also possible for the c-type of fermion irreps (see Table I in [12] for a complete list of such double point groups), but not for all the remaining cases, where the excitation manifold cannot be made complete without including explicitly some higher excitations. To illustrate the latter, consider a threelevel doublet model $|\Phi_0\rangle = |uii\rangle$, where u and its partner \bar{u} belong to the same column of an irrep (Frobenius–Schur class a) or simply different irreps (Frobenius-Schur class b). The determinants $|\Phi_0\rangle$ and $|\bar{\Phi}_0\rangle = |\bar{u}i\bar{i}\rangle$ are then not related by any point group symmetry operation and hence do not form a tensor reference. As a result, the matrix element $\langle a^{\dagger}i\Phi_0|H|a^{\dagger}\bar{i}\bar{\Phi}_0\rangle = \langle a^{\dagger}i\Phi_0|H|a^{\dagger}\bar{i}\bar{u}^{\dagger}u\Phi_0\rangle$ cannot, by virtue only of the Wigner-Eckart theorem, be reduced to a form that involves only single excitations from $|\Phi_0\rangle$. Neglecting this term will not have the correct limit of zero SOC, where the configuration $|a^{\dagger}i\bar{\Phi}_0\rangle = -|\bar{u}ai\rangle$, together with $|u\bar{a}i\rangle$ and $|ua\bar{i}\rangle$, is needed to form a spin-complete subspace for two doublets and one quartet. Therefore, for such cases, going beyond the adiabatic approximation is inevitable if one really wants to stick to a single reference $|\Phi_0\rangle$. Of course, the adiabatic approximation can still be retained if one goes to a multi-configuration version of 4C-/2C-TD-DFT by making use of 4C/2C configuration state functions (CSF). Yet, both paradigms require considerable efforts, given that even the non-relativistic counterparts [18–21] are still in their infancy.

Apart from the above technical difficulties, the jj coupling scheme for SOC is actually not of wide use as far as valence properties are concerned. It is most suited only for those elements on the *np* blocks (n > 6) of the periodic table. In contrast, the LS coupling scheme for SOC is more practical and also widely suited for typical real-life chemical systems. In this case, scalar states are first obtained by TD-DFT based on a scalar-relativistic Hamiltonian. The SOC Hamiltonian matrix over such scalar states can then be diagonalised to obtain spinor states. Such kind of 'state interaction' has a long history in the literature but was adopted first by Wang and Ziegler [22] within TD-DFT. Yet, their implementation can only handle closed-shell systems. The present account amounts to developing a composite open-shell TD-DFT approach by combing the spin-adapted TD-DFT (X-TD-DFT [3]) with the spin-free (sf) and spindependent (sd) parts [23,24] of the X2C Hamiltonian [25]. While scalar-relativistic effects are to be treated to infinite order via the sf-X2C Hamiltonian, SOC are to be treated to first order via an effective one-electron operator. The approach is to be called as sf-X2C-S-TD-DFT-SOC, see Section 2. The implementation will be described in Section 3, while the results for prototypical open-shell atomic and diatomic systems are to be discussed in Section 4. Throughout the paper, the following convention is to be employed for labelling the KS/ROKS molecular orbitals (MO): $\{i, j, k, l, \ldots\}$ for doubly occupied orbitals (closed shell part, C), $\{t, u, v, w, \ldots\}$ for singly occupied orbitals and their time-reversed partners (open shell part, O), $\{a, b, c, d, \ldots\}$ for virtual orbitals (vacant shell part, V), and $\{p, q, r, s, \ldots\}$ for unspecified orbitals. The atomic orbitals (AO) are labelled by $\{\mu, v, \kappa, \lambda, \ldots\}$. All the orbitals are assumed to be real valued since the ground-state calculations are either non-relativistic or scalar relativistic. As usual, electron spin is denoted by σ or τ . The Einstein summation convention over repeated indices is always employed.

2. Theory

2.1. The spin-adapted TD-DFT

The adiabatic U-TD-DFT amounts to solving the following non-Hermitian eigenvalue problem [11]:

$$\begin{bmatrix} \mathbf{A} & \mathbf{B} \\ \mathbf{B} & \mathbf{A} \end{bmatrix} \begin{bmatrix} \mathbf{X} \\ \mathbf{Y} \end{bmatrix} = \omega \begin{bmatrix} \mathbf{I} & \mathbf{0} \\ \mathbf{0} & -\mathbf{I} \end{bmatrix} \begin{bmatrix} \mathbf{X} \\ \mathbf{Y} \end{bmatrix}, \tag{1}$$

$$[\mathbf{A}^{\sigma\tau,\sigma'\tau'}]_{pq,rs} = \delta_{\sigma\sigma'}\delta_{\tau\tau'}(\delta_{qs}F_{pr}^{\sigma} - \delta_{pr}F_{sq}^{\tau}) + [K^{\sigma\tau,\sigma'\tau'}]_{pq,rs},$$
(2)

$$[\mathbf{B}^{\sigma\tau,\sigma'\tau'}]_{pq,rs} = [K^{\sigma\tau,\tau'\sigma'}]_{pq,sr},\tag{3}$$

where F^{σ} is the KS matrix for spin σ and the coupling matrix K is defined as

$$[K^{\sigma\tau,\sigma'\tau'}]_{pq,rs} = (p_{\sigma}q_{\tau}|s_{\tau'}r_{\sigma'}) + \left[K_{XC}^{\sigma\tau,\sigma'\tau'}\right]_{pq,rs}, \quad (4)$$

in which the second term represents the matrix elements of the XC kernel $f_{XC}^{\sigma\tau,\sigma'\tau'}$, whose explicit form depends on the chosen functional. The spin-adapted TD-DFT has been presented at length before [3,5,6]. Briefly, for flip-up excitations, X-TD-DFT [3] takes precisely the same form as U-TD-DFT albeit with ROKS orbitals. For spin-conserving excitations, X-TD-DFT [3] also takes form (1) but with the A matrix redefined as

$$\mathbf{A}(S_i) = \mathbf{A} + \Delta \mathbf{A}^{\text{RPA}},\tag{5}$$

where the correction $\Delta \mathbf{A}^{RPA}$ is just zero except for the following portions:

$$CV(\alpha\alpha) - CV(\alpha\alpha)$$
:

$$[\Delta \mathbf{A}]_{ai,bj} = \left(1 - \sqrt{\frac{S_i + 1}{S_i}} + \frac{1}{2S_i}\right) \delta_{ij} F_{ab}^S$$

$$+\left(-1+\sqrt{\frac{S_{i}+1}{S_{i}}}+\frac{1}{2S_{i}}\right)\delta_{ab}F_{ji}^{S},$$

$$CV(\alpha\alpha)-CV(\beta\beta):[\Delta\mathbf{A}]_{ai,bj}$$

$$=-\frac{1}{2S_{i}}[\delta_{ij}F_{ab}^{S}+\delta_{ab}F_{ji}^{S}],$$

$$CV(\beta\beta)-CV(\beta\beta):[\Delta\mathbf{A}]_{ai,bj}$$

$$=\left(-1+\sqrt{\frac{S_{i}+1}{S_{i}}}+\frac{1}{2S_{i}}\right)\delta_{ij}F_{ab}^{S}$$

$$+\left(1-\sqrt{\frac{S_{i}+1}{S_{i}}}+\frac{1}{2S_{i}}\right)\delta_{ab}F_{ji}^{S}.$$
(6)

Here, the symbol $CV(\alpha\alpha)$ represents an excitation from a closed-shell α orbital to a vacant-shell α orbital. The spin-polarisation matrix F^S is defined as

$$F_{pq}^{S} = \frac{1}{2} \left(F_{pq}^{\text{HF},\beta} - F_{pq}^{\text{HF},\alpha} \right) = \frac{1}{2} \sum_{t} (pt|tq),$$
 (7)

where $F^{HF,\sigma}$ is the Hartree–Fock (HF) mean-field operator for spin σ . Clearly, the implementation of X-TD-DFT is very simple. Only the one-electron terms (6) need to be added into an existing U-TD-DFT module. The calculation then proceeds precisely the same as U-TD-DFT albeit with ROKS orbitals as input. For flip-down excitations, similar corrections can also be derived but which are not considered here

To expedite the computation, Equation (1) can be recast into a form of halved dimension, viz.

$$(\mathbf{A} - \mathbf{B})(\mathbf{A} + \mathbf{B})\mathbf{Z}_I = \omega_I^2 \mathbf{Z}_I, \quad \mathbf{Z}_I = \mathbf{X}_I + \mathbf{Y}_I. \quad (8)$$

Neglecting the **B** term in Equation (1) leads to the well-known Tamm–Dancoff approximation (TDA):

$$\mathbf{A}\mathbf{X}_{I} = \omega_{I}\mathbf{X}_{I}.\tag{9}$$

It deserves to be mentioned that TDA is not only very accurate but also immune to the so-called (near) instability problem due to the decoupling between excitations and deexcitations. Therefore, it is particularly suited for studying potential energy curves with avoided crossings [3,6,26]. When an excited state is taken as the reference, as done in the so-called TRICKS-TDDFT [27] for systems with a spatially degenerate ground state, the identification of deexcitations of negative energies is much easier by TDA (9) than by the full TD-DFT (8).

2.2. The state interaction approach for SOC

In view of quasi-degenerate perturbation theory, the SOC between the spin-adapted scalar states can be treated

perturbatively through an effective Hamiltonian \mathbf{H}_{eff} ,

$$\mathbf{H}_{\text{eff}} = \Omega + \mathbf{H}_{SO},\tag{10}$$

where Ω is a diagonal matrix with the spin-free excitation energies as the diagonal elements,

$$\Omega = \operatorname{diag}\{0, \omega_1, \omega_2, \dots, \omega_N\}. \tag{11}$$

Here, the first element is for the ground state. For a degenerate ground state, there are as many zeros as the degree of degeneracy. If an excited state is taken as the reference, some ω_i will be negative. The spin—orbit matrix element between two states Ψ_I and Ψ_J reads

$$[\mathbf{H}_{SO}]_{IJ} = \langle \Psi_I | h_{SO} | \Psi_J \rangle$$

=
$$\sum_{K,I} C_{K,I} C_{L,J} \langle \Phi_K | h_{SO} | \Phi_L \rangle, \qquad (12)$$

where Φ_K and Φ_L represent the particle–hole/hole–particle transitions. The real-valued coefficients $C_{K,I}$ are the elements of the eigenvector \mathbf{X}_I (9) in TDA or \mathbf{Z}_I (8) in TD-DFT. The Hamiltonian h_{SO} considered here is an effective one-electron operator of the generic form

$$h_{SO} = \sum_{i=1}^{N} \vec{\mathbb{I}} \vec{\sigma}(i) \cdot \vec{V}(i) = \sum_{i=1}^{N} \mathbb{I} \sigma_{l}(i) V^{l}(i),$$
$$l \in \{x, y, z\}, \quad \vec{\mathbb{I}} = \sqrt{-1}, \tag{13}$$

where σ_l are the Pauli matrices and V^l real operators. The Hamiltonian can also be rewritten in second quantised form

$$h_{SO} = \sum_{pq} \left[h_{pq}^{1} T_{pq}^{\dagger}(1, -1) + h_{pq}^{0} T_{pq}^{\dagger}(1, 0) + h_{pq}^{-1} T_{pq}^{\dagger}(1, 1) \right]$$

$$(14)$$

in terms of the rank-1 tensor excitation operators

$$T_{pq}^{\dagger}(1,-1) = a_{p\beta}^{\dagger} a_{q\alpha}, \tag{15}$$

$$T_{pq}^{\dagger}(1,0) = \frac{1}{\sqrt{2}} (a_{p\alpha}^{\dagger} a_{q\alpha} - a_{p\beta}^{\dagger} a_{q\beta}),$$
 (16)

$$T_{pq}^{\dagger}(1,1) = -a_{p\alpha}^{\dagger} a_{q\beta}, \tag{17}$$

and the corresponding integrals

$$h_{pq}^{1} = h_{pq}^{\beta\alpha} = \mathbb{I}V_{pq}^{x} - V_{pq}^{y},$$
 (18)

$$h_{pq}^{0} = \sqrt{2}h_{pq}^{\alpha\alpha} = \mathbb{I}\sqrt{2}V_{pq}^{z},$$
 (19)

$$h_{pq}^{-1} = -h_{pq}^{\alpha\beta} = -\mathbb{I}V_{pq}^x - V_{pq}^y.$$
 (20)

Supposing $|\Phi_K\rangle = |\Phi_K^{SM}\rangle$ and $|\Phi_L\rangle = |\Phi_L^{S'M'}\rangle$, the matrix element $\langle \Phi_K | h_{SO} | \Phi_L \rangle$ (12) can be evaluated according to the Wigner–Eckart theorem:

$$\left\langle \Phi_K^{SM} | h_{SO} | \Phi_L^{S'M'} \right\rangle = (-1)^{S-M} \begin{pmatrix} S & 1 & S' \\ -M & M-M' & M' \end{pmatrix} \times \sum_{pq} h_{pq}^{M'-M} \left\langle \Phi_K^S \| T_{pq}^{\dagger}(1) \| \Phi_L^{S'} \right\rangle, \tag{21}$$

where the parenthesis represents the 3j symbol, while $\langle \Phi_K^S || T_{pq}^{\dagger}(1) || \Phi_L^{S'} \rangle$ is the reduced matrix element to be valued as

$$\left\langle \Phi_K^S \| T_{pq}^{\dagger}(1) \| \Phi_L^{S'} \right\rangle = \left\langle \Phi_K^{SS} | T_{pq}^{\dagger}(1, S - S') | \Phi_L^{S'S'} \right\rangle /$$

$$\left(\begin{matrix} S & 1 & S' \\ -S & S - S' & S' \end{matrix} \right).$$

$$(22)$$

For the purpose of implementation, Equation (21) can be rewritten as

$$\left\langle \Phi_K^{SM} | h_{SO} | \Phi_L^{S'M'} \right\rangle = w(S, M, S', M') \left\langle \Phi_K^{SS} | h^m | \Phi_L^{S'S'} \right\rangle, \tag{23}$$

$$w(S, M, S', M') = (-1)^{S-M} \begin{pmatrix} S & 1 & S' \\ -M & M - M' & M' \end{pmatrix} / \begin{pmatrix} S & 1 & S' \\ -M & M - M' & M' \end{pmatrix} / \begin{pmatrix} S & 1 & S' \\ -S & S - S' & S' \end{pmatrix}, \qquad (24)$$
$$\langle \Phi_K^{SS} | h^m | \Phi_L^{S'S'} \rangle = \sum_{pq} h_{pq}^m \langle \Phi_K^{SS} | T_{pq}^{\dagger} (1, S - S') | \Phi_L^{S'S'} \rangle, \\ m = M' - M = 0, \pm 1. \qquad (25)$$

The nonzero conditions for the 3j symbols in w(S, M, S', M') are $|M - M'| \le 1$ and $|S - S'| \le 1$. The latter dictates three cases for the element $\langle \Phi_K^{SS} | T_{pq}^{\dagger}(1, S - S') | \Phi_L^{S'S'} \rangle$:

$$S' = S + 1 : \langle \Phi_K^{SS} | T_{na}^{\dagger}(1, -1) | \Phi_L^{(S+1)(S+1)} \rangle, \quad (26)$$

$$S' = S : \left\langle \Phi_K^{SS} | T_{pq}^{\dagger}(1,0) | \Phi_L^{SS} \right\rangle, \tag{27}$$

$$S' = S - 1 : \langle \Phi_K^{SS} | T_{pq}^{\dagger}(1, 1) | \Phi_L^{(S-1)(S-1)} \rangle.$$
 (28)

According to the Appendix in [5], the spin-adapted basis for excited states of spin S' = S + 1 reads

$$\left|\Phi_{ex}^{(S+1)(S+1)}\right\rangle = T^{\dagger}(1,1)\left|\Phi_{0}^{SS}\right\rangle, \quad T^{\dagger} \in \{\text{CV}(1)\}, \ (29)$$

where $|\Phi_0^{SS}\rangle$ represents the ground state. The basis for excited states of spin S'=S includes two kinds of functions:

$$\left|\Phi_{ex,1}^{SS}\right\rangle = S^{\dagger}(0,0)\left|\Phi_{0}^{SS}\right\rangle, \quad S^{\dagger} \in \{\text{CO}(0), \text{OV}(0), \text{CV}(0)\},$$
(30)

$$\begin{split} \left| \Phi_{ex,2}^{SS} \right\rangle &= T^{\dagger}(1,1) \left| \Phi_{0}^{S(S-1)} \right\rangle C_{11,S(S-1)}^{SS} \\ &+ T^{\dagger}(1,0) |\Phi_{0}^{SS}\rangle C_{10,SS}^{SS}, \quad T^{\dagger} \in \{\text{CV}(1)\}, \quad (31) \end{split}$$

where $S_{pq}^{\dagger}(0,0)=\frac{1}{\sqrt{2}}(a_{p\alpha}^{\dagger}a_{q\alpha}+a_{p\beta}^{\dagger}a_{q\beta})$ is the singlet-coupled single excitation operator, and $C_{j_1m_1,j_2m_2}^{jm}=\langle j_1m_1,j_2m_2|jm\rangle$ the Clebsch–Gordan coefficient. The low-spin component $|\Phi_0^{S(S-1)}\rangle$ can be obtained from $|\Phi_0^{SS}\rangle$ by using the spin-lowering operator \hat{S}_- , i.e.

$$\left|\Phi_0^{S(S-1)}\right\rangle = \frac{1}{\sqrt{2S}}\hat{S}_{-}\left|\Phi_0^{SS}\right\rangle = \frac{1}{\sqrt{2S}}\sum_{u}a_{u\beta}^{\dagger}a_{u\alpha}\left|\Phi_0^{SS}\right\rangle. \tag{32}$$

The basis for excited states of spin S' = S - 1 can be written as

$$\begin{split} |\Phi_{ex}^{(S-1)(S-1)}\rangle &= T^{\dagger}(1,1)|\Phi_{0}^{S(S-2)}\rangle C_{11,S(S-2)}^{(S-1)(S-1)} \\ &+ T^{\dagger}(1,0)|\Phi_{0}^{S(S-1)}\rangle C_{S(S-1)}^{(S-1)(S-1)} \\ &+ T^{\dagger}(1,-1)|\Phi_{0}^{SS}\rangle C_{1(-1),SS}^{(S-1)(S-1)}, \\ &T^{\dagger} \in \{\text{OO}(1),\text{CO}(1),\text{OV}(1),\text{CV}(1)\}. \end{split}$$

Note that the symbol $\mathrm{CV}(\gamma)$ in the above bases represents a transition from a closed-shell (C) orbital to a vacant-shell (V) orbital, with $\gamma=0/1$ for singlet/triplet-coupled single excitation. Other symbols are defined similarly. After these functions are orthonormalised, the matrix element $\langle \Phi_K^{SS} | T_{pq}^{\dagger}(1, S - S') | \Phi_L^{S'S'} \rangle$ can simply be evaluated with the Slater–Condon rule for these CSF are just fixed linear combinations of Slater determinants (see Section 3).

2.3. The relativistic Hamiltonian

The above state interaction approach can be combined with any relativistic Hamiltonian that can be separated into spin-free and spin-dependent parts. In this regard, the sf-X2C+so-DKHn ($n=1,2,3,\ldots$) Hamiltonian [23,24], derived recently from the spin separation of the algebraic X2C Hamiltonian [25] in a Douglass–Kroll–Hess (DKH) fashion, is probably the best choice, as it treats scalar-relativistic effects to infinite order whereas SOC to any desired finite order n. For valence electron properties under concern here, the full sf-X2C-so-DKHn Hamiltonian can be further simplified by neglecting the two-electron scalar-relativistic interactions, the first-order spin–spin interaction, as well as the second- and higher-order spin-dependent terms therein, leading to

$$H = H_{sf} + H_{sd}, (34)$$

$$H_{sf} = \sum_{pq} [\mathbf{h}_{+,sf}^{X2C}]_{pq} a_p^{\dagger} a_q + \frac{1}{2} \sum_{pqrs} (pr|qs) a_p^{\dagger} a_q^{\dagger} a_s a_r,$$
(35)

$$H_{sd} = \sum_{pq} ([\mathbf{h}_{SO,1e}]_{pq} + [\mathbf{f}_{SO,2e}]_{pq}) a_p^{\dagger} a_q.$$
 (36)

Note that a mean-field treatment of the two-electron spinorbit interactions [24] is also assumed, see the second term in Equation (36). As shown before [25], the one-electron sf-X2C Hamiltonian $\mathbf{h}_{+,sf}^{\mathrm{X2C}}$ (35) can be obtained in one step by block-diagonalising the matrix Dirac equation. The result is

$$\mathbf{h}_{+,sf}^{\mathrm{X2C}} = \mathbf{R}_{+,0}^{\dagger} \Big(\mathbf{V}_{ne} + \mathbf{T} \mathbf{X}_{0}^{\dagger} + \mathbf{X}_{0}^{\dagger} \mathbf{T} + \mathbf{X}_{0}^{\dagger} \Big[\frac{\alpha^{2}}{4} \mathbf{W}_{sf} - \mathbf{T} \Big] \mathbf{X}_{0} \Big) \mathbf{R}_{+,0}, \qquad (37)$$

$$\mathbf{R}_{+,0} = (\mathbf{S}^{-1}\tilde{\mathbf{S}}_{+,0})^{-\frac{1}{2}} = \mathbf{S}^{-\frac{1}{2}} (\mathbf{S}^{-\frac{1}{2}}\tilde{\mathbf{S}}_{+,0}\mathbf{S}^{-\frac{1}{2}})^{-\frac{1}{2}}\mathbf{S}^{\frac{1}{2}}, \quad (38)$$

$$\tilde{\mathbf{S}}_{+,0} = \mathbf{S} + \frac{\alpha^2}{2} \mathbf{X}_0^{\dagger} \mathbf{T} \mathbf{X}_0, \tag{39}$$

where α is the fine-structure constant, **S**, **T** and \mathbf{V}_{ne} are the respective non-relativistic metric, kinetic energy and nuclear attraction (V_{ne}) , whereas \mathbf{W}_{sf} the matrix of the relativistic operator $W_{sf} = \vec{p} \cdot V_{ne} \vec{p}$. The \mathbf{X}_0 matrix is simply the ratio between the coefficients of the small and large components of the Dirac spinors of positive energies, viz.

$$\mathbf{X}_0 = \mathbf{B}_{+} \mathbf{A}_{+}^{-1} = \mathbf{B}_{+} \mathbf{A}_{+}^{\dagger} (\mathbf{A}_{+} \mathbf{A}_{+}^{\dagger})^{-1}. \tag{40}$$

With the so-obtained decoupling matrix \mathbf{X}_0 and the renormalisation matrix $\mathbf{R}_{+,0}$, the terms in H_{sd} can readily be constructed [23,24]

$$\mathbf{h}_{SO,1e} = \frac{\alpha^2}{4} \mathbf{R}_{+,0}^{\dagger} \mathbf{X}_0^{\dagger} \mathbf{W}_{SO} \mathbf{X}_0 \mathbf{R}_{+,0}, \tag{41}$$

$$\mathbf{f}_{SO,2e} = \frac{\alpha^2}{4} \mathbf{R}_{+,0}^{\dagger} [\mathbf{G}_{SO}^{LL} + \mathbf{G}_{SO}^{LS} \mathbf{X}_0 + \mathbf{X}_0^{\dagger} \mathbf{G}_{SO}^{SL} + \mathbf{X}_0^{\dagger} \mathbf{G}_{SO}^{SS} \mathbf{X}_0] \mathbf{R}_{+,0}. \tag{42}$$

Here, \mathbf{W}_{SO} is the matrix of $W_{SO} = \mathbb{I}\vec{\sigma} \cdot (\vec{p} V_{ne} \times \vec{p})$, which can be re-expressed as

$$W_{SO} = \mathbb{I}\vec{\sigma} \cdot \vec{w} = \mathbb{I}\sigma_l w^l, \quad l \in \{x, y, z\}, \tag{43}$$

$$w^{l} = \varepsilon_{lmn} p_{m} V_{ne} p_{n}, \quad w^{l}_{\mu\nu} = \varepsilon_{lmn} \langle \mu_{m} | V_{ne} | \nu_{n} \rangle = -w^{l}_{\nu\mu},$$

$$\mu_{m} = \partial_{m} \mu, \qquad (44)$$

where ε_{lmn} is the Levi-Civita symbol. $\mathbf{G}_{SO}^{XY}(X,Y \in \{L,S\})$ in Equation (42) are the matrices of the effective one-electron operator G_{SO}^{XY} ,

$$G_{SO}^{XY} = \mathbb{I}\vec{\sigma} \cdot \vec{g}^{XY} = \mathbb{I}\sigma_{l}g^{XY,l}, \quad X, Y \in \{L, S\}, \ l \in \{x, y, z\},$$
(45)

$$g_{\mu\nu}^{LL,l} = -2K_{\lambda\mu,\kappa\nu}^l P_{\lambda\kappa}^{SS},\tag{46}$$

$$g_{\mu\nu}^{LS,l} = -\left(K_{\mu\lambda,\kappa\nu}^l + K_{\lambda\mu,\kappa\nu}^l\right) P_{\lambda\kappa}^{LS},\tag{47}$$

$$g_{\mu\nu}^{SS,l} = -2\left(K_{\mu\nu,\kappa\lambda}^l + K_{\mu\nu,\lambda\kappa}^l - K_{\mu\lambda,\nu\kappa}^l\right) P_{\lambda\kappa}^{LL}, \quad (48)$$

where the two-electron integrals $K^l_{\mu\nu,\kappa\lambda}$ are defined as

$$K_{\mu\nu,\kappa\lambda}^{l} = \varepsilon_{lmn}(\mu_{m}\nu|\kappa_{n}\lambda) = -K_{\kappa\lambda,\mu\nu}^{l},$$

$$\mu_{m} = \partial_{m}\mu, \quad l, m, n \in \{x, y, z\},$$
(49)

which are antisymmetric with respect to particle interchange. Note that the terms in Equation (47) and the first two terms in Equation (48) arise from the Coulomb interaction and represent the so-called spin–same-orbit coupling, whereas the term (46) and the third term of Equation (48) originate from the Gaunt interaction and hence represent the spin–other-orbit coupling [24]. The spin-averaged density matrices \mathbf{P}^{XY} are constructed as

$$\mathbf{P}^{LL} = \mathbf{R}_{+,0} \mathbf{P} \mathbf{R}_{+,0}^{\dagger}, \quad \mathbf{P}^{LS} = \mathbf{P}^{LL} \mathbf{X}_{0}^{\dagger}, \quad \mathbf{P}^{SS} = \mathbf{X}_{0} \mathbf{P}^{LL} \mathbf{X}_{0}^{\dagger},$$
(50)

where **P** is the scalar-relativistic, spin-averaged SCF (self-consistent field) or correlated density matrix. In view of Equations (43) and (45), Equation (36) can be recast into the form of Equation (13) by introducing the following quantities:

$$\mathbf{V}^{l} = \mathbf{V}_{SO,1e}^{l} + \mathbf{V}_{SO,2e}^{l}, \quad l \in \{x, y, z\},$$
 (51)

$$\mathbf{V}_{SO,1e}^{l} = \frac{\alpha^{2}}{4} \mathbf{R}_{+,0}^{\dagger} \mathbf{X}_{0}^{\dagger} \mathbf{w}^{l} \mathbf{X}_{0} \mathbf{R}_{+,0} = -(\mathbf{V}_{SO,1e}^{l})^{T}, \quad (52)$$

$$\mathbf{V}_{SO,2e}^{l} = \frac{\alpha^{2}}{4} \mathbf{R}_{+,0}^{\dagger} [\mathbf{g}^{LL,l} + \mathbf{g}^{LS,l} \mathbf{X}_{0} + \mathbf{X}_{0}^{\dagger} \mathbf{g}^{SL,l} + \mathbf{X}_{0}^{\dagger} \mathbf{g}^{SS,l} \mathbf{X}_{0}] \mathbf{R}_{+,0} = -(\mathbf{V}_{SO,2e}^{l})^{T}.$$
 (53)

In view of the relation $(\mathbf{P}^{XY})^T = \mathbf{P}^{YX}$ (X, Y = L, S) as well as the antisymmetry property of K^l (49), we have $(\mathbf{g}^{XY,l})^T = -\mathbf{g}^{YX,l}$. Therefore, $\mathbf{V}^l_{SO,2e}$ is antisymmetric, just like $\mathbf{V}^l_{SO,1e}$. This further implies that the expectation value of H_{sd} (36) over a single determinant is just zero.

Further approximations to $\mathbf{f}_{SO,2e}$ (42) are still possible. If both \mathbf{X}_0 and $\mathbf{R}_{+,0}$ are set to unit, $\mathbf{f}_{SO,2e}$ will reduce naturally to the mean-field treatment of the two-electron Breit–Pauli (BP) spin–orbit Hamiltonian as done by Hess et al. [28]. However, the BP Hamiltonian should, in principle, be used only with non-relativistic wave functions but not with the sf-X2C ones. In view of the short-range nature

of spin-orbit interactions, the one-centre approximation to the integrals $K_{\mu\nu,\kappa\lambda}^l$ (49) can be invoked with little loss of accuracy [28,29]. In this case, only the atomic blocks of the molecular density matrix \mathbf{P}^{XY} contribute to \mathbf{G}_{SO}^{XY} . Yet, $\mathbf{f}_{SO,2e}$ is still a full matrix if no approximation is adopted for X_0 and \mathbf{R}_{+0} . Due to partial cancellations of the multi-centre one- and two-electron terms [29], the one-electron integrals (44) can also be restricted to one-centres, especially for light elements. The molecular density matrix P can be further approximated as a superposition of the atomic ones obtained from spherically averaged, non-polarised atomic SCF calculations with predetermined valence shell occupations [30]. Detailed comparisons of such approximations to $\mathbf{f}_{SO,2e}$ will be reported elsewhere [24]. Here, we just employ the spinaveraged molecular density matrix $\mathbf{P} = \frac{1}{2}(\mathbf{P}_{\alpha} + \mathbf{P}_{\beta})$, with \mathbf{P}_{α} and \mathbf{P}_{β} being the converged sf-X2C-ROKS spin density matrices, as well as the one-centre approximation to the two-electron integrals $K^l_{\mu\nu,\kappa\lambda}$. Given such approximations to the SOC Hamiltonian, the resulting errors are still much smaller than the exchange-correlation errors inherent in the approximate XC functionals/kernels as well as the spin-orbital relaxation effects not accounted for in the state interaction calculation.

The main features of the present sf-X2C-S-TD-DFT-SOC approach can be summarised as follows: (1) The common set of orthornormal orbitals is used for all states of different spin. (2) The excitation manifolds are almost singles except for those higher excitations required by spin symmetry, as viewed from the single determinant reference. (3) Both the spin-same-orbit and spin-other-orbit interactions can be treated in a unified manner, albeit at the mean-field level. (4) Since the expansion coefficients of the TD-DFT scalar states are usually very sparse, an efficient screening can be made such that thousands of scalar states can readily be handled. (5) While the sf-X2C Hamiltonian is an integrated part of TD-DFT, the present treatment of SOC is more akin to wave-function-based methods and hence goes beyond the domain of TD-DFT. That is why sf-X2C-S-TD-DFT-SOC has been termed a 'composite approach'.

3. Implementation and computational details

The previous description of the composite approach sf-X2C-S-TD-DFT-SOC is completely general. Yet, since only systems of a single unpaired electron are investigated here just to reveal the performance of the approach, only states of spin $S' = S = \frac{1}{2}$ and $S' = S + 1 = \frac{3}{2}$ need to be considered. To calculate their fine structures, the matrix elements $\langle \Phi_K^{SS} | h^m | \Phi_L^{S'S'} \rangle$ (25) can, in view of Equations (29)–(31), be evaluated in terms of the following five orthonormal high-spin CSF:

$$\begin{aligned}
&\left\{\left|\Phi_{ai,1}^{SS}\right\rangle, \left|\Phi_{ui,1}^{SS}\right\rangle = \left|\Phi_{\bar{i}}^{\bar{u}}\right\rangle, \left|\Phi_{au,1}^{SS}\right\rangle \\
&= \left|\Phi_{u}^{a}\right\rangle, \left|\Phi_{ai,2}^{SS}\right\rangle, \left|\Phi_{ai}^{(S+1)(S+1)}\right\rangle = -\left|\Phi_{\bar{i}}^{a}\right\rangle\right\}, \quad (54)
\end{aligned}$$

Table 1. Expressions for the upper triangular part of the matrix $\langle \Phi_K^{SS} | h^m | \Phi_L^{S'S'} \rangle$ (25) in the excitation manifold (54) as well as the ground state Φ_0^{SS} .

No.	Matrix elements
1	$\langle \Phi_0^{SS} h^m \Phi_0^{SS} \rangle = 0$
2	$\langle \Phi_0^{SS} h^m \Phi_{bi,1}^{SS} \rangle = 0$
3	$\langle \Phi_0^{SS} h^m \Phi_{vj,1}^{SS} \rangle = -\frac{1}{\sqrt{2}} h_{jv}^m$
4	$\langle \Phi_0^{SS} h^m \Phi_{bv,1}^{SS} angle = rac{1}{\sqrt{2}} h_{vb}^m$
5	$\langle \Phi_0^{SS} h^m \Phi_{bj,2}^{SS} angle = - \sqrt{rac{S}{1+S}} h_{jb}^m$
6	$\langle \Phi_0^{SS} h^m \Phi_{hi}^{(S+1)(S+1)} \rangle = -h_{ih}^m$
7	$\langle \Phi_{i,i,1}^{SS} h^m \Phi_{i,i,1}^{SS} \rangle = 0$
8	$\langle \Phi_{ai}^{SS} h^m \Phi_{vi}^{SS} \rangle = -\frac{1}{2} h_{av}^m \delta_{ij}$
9	$\langle \Phi_{ai,1}^{SS} h^m \Phi_{vi,1}^{SS} \rangle = -\frac{1}{2} h_{av}^m \delta_{ij}$ $\langle \Phi_{ai,1}^{SS} h^m \Phi_{bv,1}^{SS} \rangle = -\frac{1}{2} h_{vj}^m \delta_{ab}$
10	$\langle \Phi_{ai,1}^{SS} h^m \Phi_{bj,2}^{SS} \rangle = -\sqrt{\frac{S}{2(1+S)}} (h_{ab}^m \delta_{ij} - \delta_{ab} h_{ji}^m)$
11	$\langle \Phi_{ai,1}^{SS} h^m \Phi_{bj}^{(S+1)(S+1)} \rangle = -\frac{1}{\sqrt{2}} (h_{ab}^m \delta_{ij} - \delta_{ab} h_{ji}^m)$
12	$\langle \Phi_{\cdots i}^{SS} h^m \Phi_{\cdots i}^{SS} \rangle = -\frac{1}{\sqrt{\epsilon}} (h_{\cdots}^m \delta_{ij} - \delta_{uv} h_{\cdots}^m)$
13	$\langle \Phi_{ui,1}^{SS} h^m \Phi_{bv,1}^{SS} \rangle = 0$
14	$\langle \Phi^{SS}_{ui,1} h^m \Phi^{SS}_{bj,2} \rangle = \frac{1-S}{2\sqrt{S(1+S)}} h^m_{ub} \delta_{ij}$
15	$\langle \Phi^{SS}_{ui,1} h^m \Phi^{(S+1)(S+1)}_{hi} \rangle = -h^m_{ub} \delta_{ij}$
16	$\langle \Phi_{au,1}^{SS} h^m \Phi_{bv,1}^{SS} \rangle = \frac{1}{\sqrt{2}} (h_{ab}^m \delta_{uv} - \delta_{ab} h_{vu}^m)$
17	$\langle \Phi^{SS}_{au,1} h^m \Phi^{SS}_{bj,2} angle = - rac{1-S}{2\sqrt{S(1+S)}} \delta_{ab} h^m_{ju}$
18	$\langle \Phi_{au,1}^{SS} h^m \Phi_{bj}^{(S+1)(S+1)} \rangle = \delta_{ab} h_{ju}^m$
19	$\langle \Phi_{ai,2}^{SS} h^m \Phi_{bj,2}^{SS} \rangle = \frac{1}{\sqrt{2}(1+S)} (h_{ab}^m \delta_{ij} + \delta_{ab} h_{ji}^m)$
20	$\langle \Phi_{ai,2}^{SS} h^m \Phi_{bj}^{(S+1)(S+1)} \rangle = -\sqrt{\frac{s}{2(1+s)}} (h_{ab}^m \delta_{ij} + \delta_{ab} h_{ji}^m)$
21	$\langle \Phi_{ai}^{(S+1)(S+1)} h^m \Phi_{bj}^{(S+1)(S+1)} \rangle = \frac{1}{\sqrt{2}} (h_{ab}^m \delta_{ij} + \delta_{ab} h_{ji}^m)$

where

$$|\Phi_{ai,1}^{SS}\rangle = \frac{1}{\sqrt{2}}(|\Phi_i^a\rangle + |\Phi_{\bar{i}}^{\bar{a}}\rangle), \tag{55}$$

$$|\Phi_{ai,2}^{SS}\rangle = \sqrt{\frac{S}{2(1+S)}}(-|\Phi_i^a\rangle + |\Phi_{\bar{i}}^{\bar{a}}\rangle - \frac{1}{S}\sum_{u}^{2S}|\Phi_{\bar{i}u}^{a\bar{u}}\rangle). \tag{56}$$

It is curious here whether the ground state $|\Phi_0^{SS}\rangle$ can also be included in the diagonalisation of the SOC Hamiltonian matrix. Likely, this is only so when the SOC is rather weak in the ground state (vide post). For completeness, the matrix elements $\langle \Phi_K^{SS} | h^m | \Phi_L^{S'S'} \rangle$ (25) are documented explicitly in Table 1. Note in passing that the manifold (54) will reduce to $\{|\Phi_{ai,1}^{00}\rangle, |\Phi_{ai}^{11}\rangle\}$ for a closed-shell system. As for the Hamiltonian matrix elements $\langle \Phi_K^{SM} | h_{SO} | \Phi_L^{S'M'} \rangle$ (23), apart from the restrictions on the spin, i.e. $|S-S'| \leq 1$ and $|M-M'| \leq 1$, spatial symmetries can also be imposed. That is, the direct product $\Gamma_K \otimes \Gamma_L \otimes \Gamma_I$ should contain the totally symmetric irrep. Here, Γ_I (I=x,y,z) is the irrep of the Ith component of the orbital angular momentum. Although arbitrary order point group symmetries [12] have already been available in the BDF package [31–34], the calculations here made use only of D_{2h} and its subgroups,

as the implementation of sf-X2C-S-TD-DFT-SOC was for the time being based on the existing modules, including ROKS and S-TD-DFT [3,6,26].

The XC functionals considered here include SVWN5 [35], BLYP [36,37], B3LYP [38,39], BHandHLYP [36–38], CAM-B3LYP [40], and pure HF, which are featured by an increased amount of long-range exact exchange. The full XC kernels were employed for spin-conserving excitations, whereas the ALDA0 kernel [26] was used for spin-flip excitations. The latter amounts to neglecting the spin-density gradients in the spin-flip non-collinear kernel [41,42] and hence stays in the spirit of adiabatic LDA (ALDA). This particular choice is to avoid numerical instabilities associated with spin-flip transitions (for more details see [26]). The Bast basis sets [13] were used for Zn to Hg and their cations, while the uncontracted ANO-RCC triple-zeta basis sets [43–45] were employed for all other atoms.

4. Results and discussion

4.1. Closed-shell systems

Before going to open-shell systems, the performance of sf-X2C-S-TD-DFT-SOC should first be calibrated for well-behaved closed-shell systems by taking 4C-TD-DFT [8,9,13] as the benchmark. For this reason, the $ns \rightarrow np$ excitations of group 12 atoms (n = 4-6 for Zn, Cd and Hg) were calculated with the SVWN5 functional and the basis sets used by Bast [13], with the results given in Table 2. The very first question here is what and how many scalarexcited states should be included in the interaction space for spin-orbit splittings of the $^{1,3}P$ states. This can usually be guided by the symmetries and energies of the states, which can quickly be estimated by looking at the symmetries and energy levels of the corresponding occupied and virtual orbitals. The numbers of states belonging to every irrep can then readily be determined for systems of a sparse virtual orbital spectrum. Yet, to make the computation as easy as possible, we here simply set the same number (N) of states for each irrep of D_{2h} . It is seen from Table 2 that N=1, corresponding to the configuration ns^1np^1 , is already sufficient for Zn and Cd, reflecting the rather weak SOC therein. However, the situation is different for Hg, where the number of states in each irrep should be around 70 to make the fine structures converge. It is seen that the converged sf-X2C-S-TD-DFT-SOC results are in very good agreement with the corresponding 4C-TD-DFT results [13], except for the ${}^{3}P_{0}$ and ${}^{1}P_{1}$ states of Hg, where the deviations amount to -0.05 eV (or -1%). The same deviations, not reported though, were also observed for other kinds of XC functional including BLYP, B3LYP and CAM-B3LYP. This should not be surprising, as SOC is heavily dominated by the effective one-electron terms. In other words, the two-electron fluctuating SOC potential is negligibly small. It was further confirmed that switching off the spin-other-orbit coupling

Table 2. Comparison between sf-X2C-TD-DFT-SOC/LDA and 4C-TD-DFT/LDA for the $ns \to np$ excitation energies (in eV) of Zn to Hg. The interaction space for spin—orbit couplings includes N scalar states in every irrep of D_{2h} . MD and MAD: maximum and mean absolute deviations from 4C-TD-DFT [13].

				sf-X	(2C-TD-D	FT-SOC					
Atom	State	N=1	<i>N</i> =10	N=30	N=50	N=70	N=100	N=150	4C-TD-DFT ^{a/b}	4C-TD-DFT ^c	Exp^d
Zn	$^{1}S_{0}$	0.00	0.00	0.00	-0.02	-0.05	-0.09	-0.24			
	${}^{3}P_{0}$	4.32	4.32	4.32	4.32	4.32	4.32	4.32	4.32/4.37	4.32	4.01
	$^{3}P_{1}$	4.35	4.35	4.35	4.35	4.35	4.35	4.35	4.35/4.40	4.35	4.03
	$^{3}P_{2}$	4.40	4.40	4.40	4.40	4.40	4.40	4.40	4.40/4.45	4.40	4.08
	${}^{1}P_{1}$	5.76	5.76	5.76	5.76	5.76	5.76	5.76	5.77/6.07	5.76	5.80
	MD	0.00	0.00	0.00	0.00	0.00	0.00	0.00			
	MAD	0.00	0.00	0.00	0.00	0.00	0.00	0.00			
Cd	${}^{1}S_{0}$	0.00	0.00	-0.01	-0.06	-0.10	-0.24	-0.45			
	$^{3}P_{0}$	3.95	3.95	3.95	3.95	3.94	3.94	3.94	3.96/3.97	3.95	3.73
	${}^{3}P_{1}$	4.02	4.02	4.02	4.02	4.01	4.01	4.01	4.03/4.04	4.02	3.80
	$^{3}P_{2}$	4.17	4.17	4.17	4.17	4.16	4.16	4.16	4.18/4.19	4.17	3.95
	${}^{1}P_{1}$	5.34	5.34	5.34	5.34	5.34	5.34	5.34	5.47/5.50	5.34	5.42
	MD	0.00	0.00	0.00	0.00	0.00	0.00	0.00			
	MAD	0.00	0.00	0.00	0.00	0.00	0.00	0.00			
Hg	$^{1}S_{0}$	0.00	0.00	-0.10	-0.40	-1.03	-1.03	-2.34			
	$^{3}P_{0}$	4.97	4.95	4.92	4.88	4.82	4.82	4.82	4.88/4.89	4.87	4.67
	${}^{3}P_{1}$	5.17	5.16	5.13	5.10	5.05	5.05	5.05	5.10/5.12	5.08	4.89
	$^{3}P_{2}$	5.67	5.66	5.66	5.65	5.64	5.64	5.64	5.68/5.69	5.67	5.46
	${}^{1}P_{1}^{-}$	6.52	6.52	6.51	6.50	6.49	6.49	6.49	6.54/6.66	6.53	6.70
	MD	0.10	0.08	0.05	-0.03	-0.05	-0.05	-0.05			
	MAD	0.05	0.04	0.03	0.02	0.04	0.04	0.04			

^aA set of diffuse spd Slater functions was further augmented to the basis sets used in [9]

in $\mathbf{f}_{SO,2e}$ (42), not considered in the 4C-TD-DFT calculations [13], does not change the present results discernibly (less than 0.005 eV). Therefore, the major source of error for SOC is due to the spin-orbital relaxation effects not accounted for by sf-X2C-S-TD-DFT-SOC. This can actually be expected in view of the interaction matrix elements shown in lines 11 and 21 in Table 1. The SOC between the excited singlet and triplet states involve rotations among the occupied and virtual orbitals separately, but no rotations between the occupied and virtual ones. Only the latter represent spin-orbital relaxations. To get such effects, spinfree double excitations would be required but which cannot be captured by adiabatic TD-DFT. It sounds like that the Brillouin conditions between the spin-free ground state and the excited spinor states are retained by sf-X2C-S-TD-DFT-SOC.

The next question is whether the spin-free ground state can be included in the interaction space, so as to capture the SOC also of the ground state. Since the matrix elements between the ${}^{1}S$ and 1 , ${}^{3}P$ states vanish due to symmetry reason, including ${}^{1}S$ in the interaction space of a given dimension does not affect the excitation energies of the excited spinor states with respect to ${}^{1}S$. Yet, as seen from Table 2, the energy of ${}^{1}S_{0}$ becomes increasingly lower as the interac-

tion space is enlarged, to a much larger extent than the excited spinor states. While the latter is due to the lack of spin-orbital relaxations, the former does arise from such effects as the interaction matrix elements (line 6 in Table 1) do involve rotations between the occupied and virtual orbitals. If all the scalar-excited states are included in the interaction space, the diagonalisation would be equivalent to a single SOC-SCF cycle after the sf-X2C-SCF has converged, which would be close to the converged X2C-SCF only when the SOC in the ground state is rather weak. However, this is not the case for the ground states of Zn to Hg. More specifically, the so-obtained SOC of ¹S are far away from the true differences between the X2C-LDA and sf-X2C-LDA ground-state energies, which are -0.02, -0.52 and -20.6 a.u. for Zn, Cd and Hg, respectively. This exercise reveals that including the ground state in the SOC interaction space is generally not meaningful, although it may occasionally provide reasonable results when confined to a small interaction space (vide post).

An additional remark is in order. It appears that a good description of the ${}^{1}P_{1}$ states of Zn to Hg requires the use of diffuse functions. By adding one set of diffuse spd Slater functions to the mixed numerical and Slater basis sets employed in the previous 4C-TD-DFT calculations [8], the

^bRef. [9].

^cRef. [13].

^dRef. [46].

Downloaded by [Washington University in St Louis] at 00:13 06 October 2014

Table 3. Low-lying excited states of Zn⁺, Cd⁺ and Hg⁺. For each functional, the two columns refer to the sf-X2C-S-TDA energies (in eV) with and without SOC, respectively. The spin—orbit splittings are further displayed in parentheses. EOMIP: shorthand notion for SOC-EOMIP-CCSD (see the text). MD and MAD: maximum and mean absolute deviations from experiment.

						8	f-X2C-S-	sf-X2C-S-TDA with and without SOC	and with	out SOC						
Atom	Term	J	SVV	SVWN5	BLYP	7.P	B3LYP	XP	CAM-B3LYP	33LYP	BHandHLYP	HLYP	H	HF	EOMIP^a	$\mathrm{Exp.}^b$
Zn^+	$^{2}P\left[3d^{10}4p ight]$	-12	6.85	6.93	6.84	6.92	6.61	89.9	6.49	95.9	6.29	6.36	5.43	5.49	6.83	6.01
		wl0	96.9	(0.11)	6.95	(0.11)	6.72	(0.10)	09.9	(0.11)	6:39	(0.10)	5.52	(0.09)	6.93(0.09)	6.12(0.11)
	$^{2}D\left[3d^{9}4s^{2} ight]$	v10	6.07	6.20	5.75	5.88	6.62	6.75	09.9	6.73	7.82	7.94	10.09	10.22	7.89	7.78
		w17	6:39	(0.32)	6.07	(0.31)	6.94	(0.31)	6.92	(0.31)	8.13	(0.31)	10.40	(0.30)	8.20 (0.32)	8.11 (0.34)
	$^{2}S[3d^{10}5s]$	717	11.17	11.17	10.86	10.86	10.89	10.89	10.97	10.97	10.74	10.74	10.13	10.13		10.96
	$^{2}D\left[3d^{10}4d ight]$	ı 610	12.16	12.17	11.84	11.84	11.85	11.85	11.98	11.99	11.71	11.72	11.13	11.13		12.02
		wl0	12.17	(0.01)	11.84	(0.01)	11.85	(0.01)	11.99	(0.01)	11.72	(0.01)	11.13	(0.00)		12.02 (0.01)
	$^{2}P\left[3d^{10}5p ight]$	-17	12.28	12.30	11.95	11.97	12.18	12.19	12.08	12.04	12.13	12.15	11.71	11.73		12.57
		w17	12.32	(0.04)	11.99	(0.03)	12.20	(0.02)	12.11	(0.02)	12.16	(0.03)	11.73	(0.03)		12.60 (0.03)
Cq+	$^{2}P\left[4d^{10}5p ight]$	717	6.10	6.31	6.07	6.27	5.87	6.07	5.70	5.90	5.57	5.77	4.75	4.92	6.50	5.47
		w 0	6.41	(0.31)	6.36	(0.29)	6.16	(0.29)	00.9	(0.31)	5.86	(0.29)	5.01	(0.26)	6.77 (0.27)	5.78 (0.31)
	$^{2}D[4d^{9}5s^{2}]$	νI0	7.36	7.63	7.16	7.43	7.75	8.02	7.79	8.05	8.54	8.80	68.6	10.00	8.71	8.59
		wl0	8.03	(0.66)	7.82	(0.66)	8.41	(0.65)	8.45	(0.66)	9.18	(0.65)	10.65	(0.76)	9.39 (0.68)	9.29 (0.70)
	^{2}S [4 $d^{10}6s$]	-12	10.37	10.37	10.00	10.00	10.06	10.06	10.11	10.11	9.93	9.93	9.28	9.28		10.29
	$^{2}D[4d^{10}5d]$	wl0	11.13	11.14	10.75	10.76	10.80	10.81	10.90	10.91	10.69	10.70	10.03	10.31		11.12
		v10	11.15	(0.02)	10.77	(0.02)	10.82	(0.02)	10.92	(0.02)	10.71	(0.02)	10.17	(0.14)		11.14 (0.02)
	$^{2}P\left[4d^{10}6p ight]$	-12	11.53	11.57	11.07	11.11	11.23	11.28	11.38	11.43	11.17	11.22	10.67	10.72		11.74
		wl0	11.59	(0.07)	11.13	(0.06)	11.30	(0.07)	11.45	(0.08)	11.24	(0.07)	10.74	(0.07)		11.83 (0.08)
Hg^{+}	$^{2}D[5d^{9}6s^{2}]$	213	3.60	4.32	3.46	4.18	3.87	4.59	3.92	4.64	4.42	5.14	5.38	60.9	4.41	4.40
		ωl0	5.41	(1.81)	5.26	(1.79)	99.5	(1.79)	5.72	(1.80)	6.21	(1.79)	7.15	(1.77)	6.23 (1.83)	6.27 (1.86)
	$^{2}P\left[5d^{10}6p ight]$	-12	7.01	7.78	6.94	7.67	6.75	7.50	6.52	7.30	6.45	7.19	5.60	6.31	7.97	6.38
		wl0	8.09	(1.08)	7.97	(1.03)	7.81	(1.05)	7.63	(1.10)	7.51	(1.06)	6.61	(1.01)	9.02 (1.05)	7.51 (1.13)
	$(^2D_{\frac{5}{2}}, ^3P_0)$ [5 d^96s6p]	213	9.11	10.59	86.8	10.42	9.28	10.73	9.11	10.60	9.64	11.07	9.70	11.02		88.6
	$(^2D_{\frac{5}{2}}, ^3P_1)$ [5 d^9 6s6 p]	r-12	9.49	10.72	9.31	10.53	6.67	10.89	9.53	10.76	10.11	11.30	10.42	11.44		10.44
		νI0	9.73	(0.24)	9.54	(0.23)	9.87	(0.19)	9.72	(0.19)	10.26	(0.14)	10.48	(0.06)		10.52 (0.08)
		۳I7	9.84	(0.11)	29.6	(0.13)	10.03	(0.16)	6.87	(0.15)	10.46	(0.20)	10.65	(0.18)		10.68 (0.17)
MD MAD			-1.73 0.64		-2.04 0.80		-1.18 0.52		-1.19 0.48		-0.58 0.24		2.32 0.90			
7																

^aRef. [47]. ^bRef. [46].

Downloaded by [Washington University in St Louis] at 00:13 06 October 2014

Table 4. Low-lying excited states (in eV) of Cu, Ag and Au. EOMEA: shorthand notation for SOC-EOMEA-CCSD (see the text). For other explanations, see Table 3.

							3	:] :	(
		'				-IS	X2C-S-1	st-X2C-S-TDA with and without SOC	and withc	out SOC							
Atom	Term	ſ	SVWN5	VNS	BI	BLYP	B3I	ВЗЦУР	CAM-	CAM-B3LYP	BHan	BHandHLYP	1	HF	$EOMIP^a$	$EOMEA^b$	$\mathrm{Exp.}^c$
Cu	$^{2}D\left[3d^{9}4s^{2} ight]$	213	69.0	0.78	0.47	0.57	1.05	1.15	1.10	1.19	1.89	1.99	3.57	3.67	2.30	6.55	1.39
		w10	0.92	(0.24)	0.71	(0.23)	1.29	(0.23)	1.33	(0.23)	2.13	(0.23)	3.80	(0.23)	2.54 (0.24)	6.83 (0.28)	1.64(0.25)
	$^2P\left[3d^{10}4p ight]$		4.24	4.25	4.12	4.12	4.07	4.09	3.96	3.99	3.82	3.84	3.08	3.09	4.23	3.73	3.79
			4.27	(0.04)	4.15	(0.03)	4.10	(0.03)	4.00	(0.04)	3.85	(0.03)	3.10	(0.03)	4.26 (0.03)	3.76 (0.03)	3.82 (0.03)
	$^{4}P\left[3d^{9}4s4p ight]$		3.95	4.04	3.82	3.92	4.47	4.57	4.51	4.60	5.38	5.48	6.28	6.37			4.84
		70 m	4.06	(0.11)	3.93	(0.10)	4.60	(0.12)	4.63	(0.13)	5.51	(0.13)	6.41	(0.13)			4.97(0.14)
		-12	4.15	(0.09)	4.02	(0.09)	4.69	(0.09)	4.73	(0.10)	5.60	(0.10)	6.52	(0.11)			5.08 (0.10)
	$^{4}F\left[3d^{9}4s4p ight]$	612	4.03	4.11	3.90	3.98	4.58	4.65	4.62	4.69	5.53	5.60	6.57	6.63			5.07
		r ₁ 2	4.05	(0.02)	3.91	(0.02)	4.59	(0.02)	4.64	(0.01)	5.55	(0.01)	09.9	(0.03)			5.10 (0.03)
		213	4.11	(0.05)	3.96	(0.04)	4.64	(0.04)	4.68	(0.04)	5.59	(0.04)	6.64	(0.04)			5.15 (0.05)
		w10	4.18	(0.08)	4.04	(0.08)	4.72	(0.09)	4.76	(0.00)	5.68	(0.09)	6.71	(0.06)			5.24 (0.09)
	$^{2}S[3d^{10}5s]$	21	5.41	5.41	5.12	5.12	5.14	5.14	5.29	5.28	4.98	4.98	4.46	4.46		5.19	5.35
Ag	$^{2}P\left[4d^{10}5p ight]$	21	4.32	4.42	4.30	4.40	4.13	4.22	3.95	4.05	3.87	3.96	3.15	3.23	4.23	3.66	3.66
		213	4.47	(0.14)	4.44	(0.14)	4.27	(0.14)	4.10	(0.15)	4.01	(0.14)	3.27	(0.12)	4.32 (0.08)	3.77 (0.11)	3.78 (0.11)
	$^{2}D[4d^{9}5s^{2}]$	ائ 2ائ	3.00	3.21	2.84	3.05	3.30	3.51	3.38	3.59	3.93	4.14	5.09	5.24	4.38	7.72	3.75
		w10	3.52	(0.52)	3.36	(0.52)	3.82	(0.52)	3.90	(0.52)	4.44	(0.51)	5.29	(0.20)	4.90(0.52)	8.23 (0.51)	4.30(0.55)
	$^{2}S[4d^{10}6s]$	717	5.45	5.45	5.15	5.15	5.18	5.18	5.24	5.24	5.04	5.04	4.49	4.49		5.23	5.28
Au	$^{2}D[5d^{9}6s^{2}]$	ائ 2ائ	0.72	1.31	0.61	1.19	0.91	1.49	0.97	1.55	1.32	1.90	2.03	2.61	1.41	5.04	1.14
		713ء	2.19	(1.47)	2.07	(1.46)	2.36	(1.46)	2.43	(1.46)	2.77	(1.45)	3.48	(1.45)	2.89 (1.48)	6.57 (1.53)	2.66 (1.52)
	$^{2}P[5d^{10}6p]$	-12	5.16	5.62	5.10	5.53	4.96	5.41	4.72	5.21	4.69	5.16	3.92	4.35	5.94	4.70	4.63
		213	5.73	(0.57)	5.61	(0.52)	5.48	(0.52)	5.32	(0.60)	5.32	(0.63)	4.52	(0.60)	6.38(0.44)	5.19 (0.49)	5.11 (0.47)
	$^{4}P\left[5d_{\frac{5}{2}}^{9}6s_{\frac{1}{2}}^{1}6p_{\frac{1}{2}}^{1}\right]$	215	4.84	5.84	4.76	5.74	4.96	5.95	4.81	5.83	5.21	6.20	5.10	6.04			5.23
	$^4F[5d_{rac{9}{5}}^96s_{rac{1}{2}}6p_{rac{1}{2}}]$	r-12	5.09	5.94	4.97	5.83	5.22	80.9	5.09	5.97	5.55	6:39	5.66	6:39			5.65
	ı	215	5.28	(0.20)	5.15	(0.18)	5.38	(0.16)	5.25	(0.15)	5.67	(0.12)	5.74	(0.08)			5.72 (0.08)
MD MAD		•	-1.06		-1.21 0.74		-0.52 0.37		-0.52 0.31		0.54		2.18				

^aRef. [47]. ^bRef. [48]. ^cRef. [46].

			sf-X2	2C-S-TDA-SOC					
Atom	SVWN5	BLYP	B3LYP	CAM-B3LYP	BHandHLYP	HF	EOM-CC	CASPT2/RASSI ^c	Exp.^d
В	0.003	0.003	0.003	0.003	0.002	0.002		0.002	0.002
Al	0.021	0.022	0.019	0.018	0.016	0.011		0.013	0.014
Ga	0.160	0.158	0.134	0.138	0.125	0.089	0.100^{a}	0.099	0.102
In	0.388	0.374	0.348	0.337	0.309	0.228	0.267^{a}	0.261	0.274
Tl	1.337	1.294	1.223	1.196	1.108	0.843	0.921^{a}	0.893	0.966
F	0.052	0.052	0.052	0.052	0.051	0.050		0.050	0.050
C1	0.117	0.116	0.114	0.114	0.111	0.103		0.102	0.109
Br	0.500	0.492	0.482	0.486	0.464	0.428	0.455^{b}	0.422	0.457
I	1.014	0.991	0.974	0.984	0.941	0.872	0.934^{b}	0.863	0.943
At	2.839	2.783	2.755	2.793	2.693	2.540	2.824^{b}	2.517	-

Table 5. Spin-orbit splittings (in eV) for the ground states ²P of groups 13 and 17 atoms.

results become virtually identical with those obtained with Gaussian basis sets [13].

As an additional test, sf-X2C-S-TD-DFT-SOC was also applied to the lowest 50 spinor states of OsO_4 . Without going into details, the maximum and mean absolute deviations from the corresponding X2C-TD-DFT results [15] amount to -0.07 and 0.03 eV, respectively. It is hence clear that sf-X2C-S-TD-DFT-SOC can safely be recommended as an alternative to the genuine 4C- or 2C-TD-DFT.

4.2. Open-shell systems

4.2.1. Open-shell systems with a spatially non-degenerate ground state

After having examined the performance of sf-X2C-S-TD-DFT-SOC for well-behaved closed-shell systems, we come to open-shell systems, among which those of a spatially non-degenerate ground state are the simplest. The cations of the group 12 atoms are such examples, where the lowest CO. OV and CV types of transitions from the ground state $(n-1)d^{10}ns^1$ will give rise to the respective $(n-1)d^9ns^2$, $(n-1)d^{10}ns^0np^1$ and $(n-1)d^9ns^1np^1$ superconfigurations. To avoid the instability problem often encountered in full TD-DFT, we use instead sf-X2C-S-TDA in the spin-free calculations. In the subsequent SOC calculations, the number of scalar states was set to 100 for every irrep of D_{2h} . The results obtained with various functionals are given in Table 3. For comparison, the excited states of Cu, Ag and Au, which are valence isoelectronic to Zn⁺, Cd⁺ and Hg⁺, were also investigated, with the results documented in Table 4. The sf-X2C-S-TDA-SOC results are to be compared with the experimental data [46] as well as the SOC-EOMIP-CCSD [47] and SOC-EOMEA-CCSD [48] values where the SOC were not included in the closed-shell reference states but included through two-component effective core potentials (ECP) in both the coupled-cluster with singles and doubles (CCSD) and equation-of-motion (EOM) steps for the ionised (IP) or electron-attached (EA) states.

It is first noted that the spin-orbit splittings obtained by the various functionals as well as SOC-EOMIP-CCSD/SOC-EOMEA-CCSD are very similar to each other, confirming again that the interplay between SOC and correlation is rather weak. Therefore, we focus mainly on the scalar states here. Noticeably, their energies vary strongly with the amount of HF exchange in the functionals, depending on the nature of the excitations. More specifically, for the OV type of excitations, including the 2P (ns $\rightarrow np$ or (n +1)p), ${}^{2}D$ (ns \rightarrow nd) and ${}^{2}S$ (ns \rightarrow (n + 1)s) states, the energies increase as the amount of HF exchange decreases from HF (100%) to BLYP (0%). However, the opposite is true for the CO or CV type of excitations. The former includes the 2D state from the $(n-1)d \rightarrow ns$ transition whereas the latter includes those predominated by the (n -1) $d \rightarrow np$ transition (see the highest states of Hg⁺ in Table 3 and of Au in Table 4). As a result, the orderings of the states may not be predicted correctly by some functionals. This is indeed the case for SVWN5 and BLYP, which yield wrong orderings for the first two states of Ag and Zn⁺ as well as the ${}^{2}P$ and ${}^{4}P$ states of Cu. So are B3LYP and CAM-B3LYP for the first two states of Ag. Overall, the BHandHLYP functional performs the best as judged from the maximum and mean absolute deviations from experiment [46]. A close inspection reveals that, among the six ions/atoms investigated here, Cu is most peculiar. The excitation energies for the transitions from 3d to 4s or 4p are overestimated by approximately 0.5 eV by BHandHLYP and even by 1 eV by SOC-EOMIP-CCSD [47]. This is likely due to the strong non-dynamical correlation between Cu3d and 4s4p, which are very close both in energy and space.

The success of sf-X2C-S-TD-DFT-SOC can be attributed to spin adaptations of both the reference and

aSOC-EOMEA-CCSD [48].

^bSOC-EOMIP-CCSD [47]

^cRef. [49].

^dRef. [46].

the excitation manifold, as well as the balanced treatment of exchange and correlation. In contrast, these factors cannot readily be built into wave-function-based single reference (SR) methods. For instance, so far there does not exist a satisfactory spin-adapted coupled-cluster approach for open-shell ground states, needless to say excited states. Approaches like SOC-EOMIP-CCSD [47] and SOC-EOMEA-CCSD [48] try to circumvent the spin-adaptation problem by selecting a closed-shell system as the reference. However, due to truncations in the correlation and excitation spaces, such approaches can only handle some special cases, usually those predominated by single excitations. For example, when starting from the neutral reference ${}^{1}S[(n-1)d^{10}ns^{2}]$, SOC-EOMIP-CCSD performs well for the single-electron ionised ${}^{2}D[(n-1)d^{9}ns^{2}]$ states of Zn^+ , Cd^+ and Hg^+ , but fails miserably for the 2P [(n -1) $d^{10}np$] states that can only be reached by simultaneously ionising and exciting the two electrons occupying ns. A similar situation also occurs to SOC-EOMEA-CCSD for Cu, Ag and Au when starting from the cationic reference ${}^{1}S[(n-1)d^{10}]$. The single-electron attached states ${}^{2}P[(n-1)d^{10}]$ 1) $d^{10}np$] are well described but the ${}^{2}D[(n-1)d^{9}ns^{2}]$ states now become the hard case due to the involvement of twoelectron attachment–excitation processes. As a result, their energies are overestimated by 4-5 eV by SOC-EOMEA-CCSD. Note in passing that unlike the case of Zn⁺, Cd⁺ and Hg⁺, the ${}^{2}D[(n-1)d^{9}ns^{2}]$ states of Cu, Ag and Au cannot really be well described even through single-electron ionisations of ${}^{1}S[(n-1)d^{10}ns^{2}]$, because the dramatic orbital relaxations of such an anionic reference cannot fully be captured by the EOM step of SOC-EOMIP-CCSD. In contrast, the so-discussed states are all well described by sf-X2C-S-TDA-SOC/BHandHLYP with very little computational efforts. However, this does not imply that TD-DFT outperforms uniformly the wave-function-based SR methods. It is just that spin adaptation as well as higher excitations must be incorporated in the latter to be worthy of the merit of 'systematic improvement'.

4.2.2. Open-shell systems with a spatially degenerate ground state

Open-shell systems with a spatially degenerate ground state are more involved than the previous examples with a spatially non-degenerate ground state. Both spatial and spin symmetries have to be incorporated explicitly into the ROKS reference and TD-DFT. Although this can in principle be done, we take instead a circuitous route here by taking a spatially non-degenerate excited state as the reference. The spin-orbit splittings of the ground state can then be assessed through de-excitations. The group 13 and 17 atoms represent such examples. The excited configurations $ns^2np^0(n+1)s^1$ and ns^1np^6 (n=2-6) can be taken as the references for B-Tl and F-At, respectively. The calculated spin-orbit splittings of the ground states,

Table 6. Equilibrium bond lengths R_e (in Å), harmonic frequencies ω_e (in cm⁻¹) and adiabatic excitation energies T_e (in eV) for the ground and excited states of HgH calculated with sf-X2C-S-TDA and sf-X2C-S-TDA-SOC using the BHandHLYP functional and the $^2\Sigma^+$ reference.

	Method	$^2\Sigma^+$	$^{2}\Pi$	
R_e	sf-X2C-S-TDA	1.741	1.578	
	CCSD^a	1.747	1.576	
	$EOMEA-CCSD^a$	1.720	1.578	
ω_e	sf-X2C-S-TDA	1437	2182	
	CCSD^a	1372	2118	
	EOMEA-CCSD a	1545	2103	
T_e	sf-X2C-S-TDA		3.14	
	CCSD^a		3.28	
	EOMEA-CCSD a		3.20	
	Method	$X^2\Sigma^+$	$A_1{}^2\Pi_{\frac{1}{2}}$	$A_2^2 \Pi_{\frac{3}{2}}$
R_e	sf-X2C-S-TDA-SOC	1.726	1.579^{2}	1.578^{2}
	SOC-EOMEA-CCSD ^a	1.706	1.580	1.577
	GRECP-FS-CCSD(13e-T) ^b	1.730	1.582	1.579
	DC-FS-CCSD(13e-T) ^c	1.753	1.597	1.594
	$\operatorname{Exp.}^d$	1.741	1.583	1.581
ω_e	sf-X2C-S-TDA-SOC	1492	2173	2180
·	SOC-EOMEA-CCSD ^a	1583	2091	2108
	GRECP-FS-CCSD(13e-T) ^b	1424	2065	2083
	DC-FS-CCSD(13e-T)c	1359	1990	2005
	$\operatorname{Exp.}^d$	1385	2068	2091
T_{ρ}	sf-X2C-S-TDA-SOC		3.09	3.53
·	SOC-EOMEA-CCSD ^a		3.00	3.44
	GRECP-FS-CCSD(13eT) ^b		3.06	3.51
	DC-FS-CCSD(13eT) ^c		3.05	3.49
	Exp.d		3.05	3.51

^aRef. [48].

through the respective $(n + 1)s \rightarrow np$ and $np \rightarrow ns$ deexcitations, are given in Table 5. It is seen that the splittings decrease slowly as the amount of HF exchange increases. Again, BHandHLYP performs the best among the tested XC functionals, with the results in good agreement with those by SOC-EOMIP/EA-CCSD [47,48] and CASPT2/RASSI (complete active space second-order perturbation theory for correlation and restricted active space state interaction for SOC) [49], as well as the experimental values [46].

4.2.3. Spectroscopic constants of HgH, PbF and I_2^+

Besides atomic systems, the present implementation of sf-X2C-S-TD-DFT-SOC is also applicable to molecular systems. The three molecules of HgH, PbF and I_2^+ are considered here as they have been extensively studied both experimentally and theoretically. The BHandHLYP functional was used in both the sf-X2C-ROKS and sf-X2C-S-TDA-SOC calculations of the molecular spectroscopic constants, including the equilibrium bond lengths R_e , harmonic frequencies ω_e , and adiabatic excitation energies T_e .

^bRef. [51]. 13eT: triple corrections for the 13 valence electrons.

^cRef. [52]

^dRef. [50].

Table 7. Equilibrium bond lengths R_e (in Å), harmonic frequencies ω_e (in cm⁻¹) and adiabatic excitation energies T_e (in eV) for the ground and excited states of PbF calculated with sf-X2C-S-TDA and sf-X2C-S-TDA-SOC using the BHandHLYP functional and the $A^2\Sigma^+$ reference.

	Method	$^{2}\Pi$	$A^2\Sigma^+$	$B^2\Sigma^{+}$	
$\overline{R_e}$	sf-X2C-S-TDA	2.041	2.188	1.983	
	CCSD^a	2.040	2.175	1.976	
	$EOMEA-CCSD^a$	2.040	2.167		
ω_e	sf-X2C-S-TDA	529	379	613	
	CCSD^a	534	386	619	
	$EOMEA^a$	532	394		
T_e	sf-X2C-S-TDA		2.16	3.80	
	CCSD^a		2.18	3.84	
	$EOMEA-CCSD^a$		2.21		
	Method	$X_1^2\Pi_{\frac{1}{2}}$	$X_2^2 \Pi_{\frac{3}{2}}$	$A^2\Sigma^+$	$B^2\Sigma$ +
R_e	sf-X2C-S-TDA-SOC	2.057^{2}	2.037^{2}	2.163	1.983
	$SOC ext{-}EOMEA ext{-}CCSD^a$	2.054	2.032	2.150	1.971
	Exp^b	2.058	2.034	2.160	1.976
ω_e	sf-X2C-S-TDA-SOC	508	534	392	614
	$SOC ext{-}EOMEA ext{-}CCSD^a$	514	536	406	620
	Exp. ^b	503	529	395	606
T_e	sf-X2C-S-TDA-SOC		1.03	2.75	4.41
-	SOC-EOMEA-CCSD ^a		0.98	2.86	4.43
	Exp^b		1.02	2.80	4.42

^aRef. [48].

The results are documented in Tables 6, 7 and 8 for HgH, PbF and I_2^+ , respectively. The ground state ${}^2\Sigma^+$ of HgH is spatially non-degenerate and can hence be taken as the reference. Compared with experiment [50], the deviations of the present results are 0.004 Å for R_e , 105 cm⁻¹ for ω_e , and less than 0.05 eV for T_e for the two excited states, and -0.015 Å for R_e and 107 cm⁻¹ for ω_e for the ground state $X^2\Sigma^+$. Such an accuracy is very similar to that achieved by the more expensive approaches such as SOC-EOMEA-CCSD [48] and FS-CCSD (Fock-space CCSD) with either the generalised relativistic ECP (GRECP) [51] or the all-electron Dirac—Coulomb (DC) Hamiltonian [52].

As for PbF, the ground state ${}^{2}\Pi$ can be written as $\sigma_{\text{F2}p}^2 \pi_{\text{Pb6}p}^1 \sigma_{\text{Pb6}p}^0 \sigma_{\text{F3}s}^0$, which is spatially degenerate. Instead, the first excited state $A^2\Sigma^+$ represented by $\sigma_{\text{F2}p}^2 \pi_{\text{Pb6}p}^0 \sigma_{\text{Pb6}p}^1 \sigma_{\text{F3}s}^0$ is spatially non-degenerate and hence suitable for the reference. The ground state is then accessed via the de-excitation $\sigma_{Pb6p} \rightarrow \pi_{Pb6p}$, while the Rydberg state $B^2\Sigma^+$ via the excitation $\sigma_{Pb6p} \to \sigma_{F3s}$. It is seen from Table 7 that the substantial spin-orbit splitting of the ground state $^{2}\Pi$ is well reproduced by sf-X2C-S-TDA-SOC. Also, the calculated spectroscopic constants for the four spinor states are in excellent agreement with the experimental results [53]. As mentioned before, including the reference in the diagonalisation of the SOC matrix is occasionally meaningful. This is indeed the case here for PbF. By including the reference $A^2\Sigma^+$ in the SOC matrix, the SOC-induced contraction in the bond length (0.025 Å) and increases in the vibrational frequency (13 cm⁻¹) and adiabatic excitation energy (0.59 eV) are well reproduced, as compared with the corresponding SOC-EOMEA-CCSD values of 0.017 Å, 12 cm⁻¹ and 0.65 eV [48].

The lowest three scalar states of I_2^+ are ${}^2\Pi_g (\sigma_g^2 \pi_u^4 \pi_g^3)$, $^{2}\Pi_{u}$ $(\sigma_{g}^{2}\pi_{u}^{3}\pi_{g}^{4})$ and $^{2}\Sigma^{+}$ $(\sigma_{g}^{1}\pi_{u}^{4}\pi_{g}^{4})$ in energetic ascending order. By choosing the ${}^2\Sigma^+$ state as the reference, the ground and first excited states can be reached by the CO type of de-excitations $\pi_g \to \sigma_g$ and $\pi_u \to \sigma_g$, respectively. Since there are no adequate experimental values [54] for the spinor states, the sf-X2C-S-TDA-SOC results are compared mainly with the SOC-EOMIP-CCSD [47] and FS-CCSD [52] values. Due to the rather weak bondings in all the states, as reflected by the very small force constants, the discrepancies between the present sf-X2C-S-TDA-SOC and the presumably most accurate DCG-FS-CCSD results are quite large, peaked at the $A^2 \prod_{\frac{3}{2}, u}$ state, where the differences amount to 0.10 Å for R_e , 33 cm⁻¹ for ω_e , and 0.19 eV for T_e . The $B^2\Sigma^+$ state was also calculated by including the ${}^{2}\Sigma^{+}$ reference in the spin-orbit interaction space. However, the results are completely out of trend. The SOC effects on R_e (+0.11 Å) and ω_e (-39 cm⁻¹) are simply too large compared with the other four spinor states resulting from ${}^{2}\Pi_{g}$ and ${}^{2}\Pi_{u}$ (-0.002 to +0.006 Å in R_{e} and -4 to +3 cm⁻¹ in ω_e). To confirm this, we further carried out X2C-SCF calculations for $B^2\Sigma^+$ and indeed found that the results ($R_e = 2.953 \text{ Å and } \omega_e = 118 \text{ cm}^{-1}$) are very different from those ($R_e = 3.109 \text{ Å}$ and $\omega_e = 81 \text{ cm}^{-1}$) by sf-X2C-S-TD-DFT-SOC. Again, this shows that the inclusion of the

^bRef. [53].

Table 8. Equilibrium bond lengths R_e (in Å), harmonic frequencies ω_e (in cm⁻¹) and adiabatic excitation energies T_e (in eV) for the ground and excited states of I_2^+ calculated with sf-X2C-S-TDA and sf-X2C-S-TDA-SOC using the BHandHLYP functional and the ${}^2\Sigma_o^+$ reference.

	Method	$^2\Pi_g$	$^{2}\Pi_{u}$	$^2\Sigma_g^+$		
$\overline{R_e}$	sf-X2C-S-TDA	2.584	2.835	2.991		
ω_e	sf-X2C-S-TDA	252	185	120		
T_e	sf-X2C-S-TDA		1.75	2.98		
	Methods	$X^{2}\prod_{\frac{3}{2},g}$	$X^{2}\Pi_{\frac{1}{2},g}$	$A^{2}\Pi_{\frac{3}{2},u}$	$A^2\Pi_{\frac{1}{2},u}$	$B^2\Sigma_g^+$
R_e	sf-X2C-S-TDA-SOC	2.583	2.590^{210}	2.837	2.833	3.109
	SOC - $EOMIP$ - $CCSD^a$	2.577	2.586	2.863	2.842	2.934
	$DC ext{-}FS ext{-}CCSD^b$	2.61	2.62	2.91	2.88	2.97
	DCG-FS-CCSD ^c	2.63	2.63	2.94	2.91	3.01
	Exp^d	_	_	_	_	_
ω_e	sf-X2C-S-TDA-SOC	253	248	185	188	81
	SOC-EOMIP-CCSD ^a	249	242	167	176	133
	$\mathrm{DC ext{-}FS ext{-}CCSD}^b$	242	233	158	168	129
	DCG-FS-CCSD ^c	235	226	152	162	121
	Exp^d	240	230	138	_	_
T_e	sf-X2C-S-TDA-SOC		0.62	1.80	2.41	3.13
	SOC-EOMIP-CCSD ^a		0.65	1.77	2.48	3.44
	$\mathrm{DC} ext{-}\mathrm{FS} ext{-}\mathrm{CCSD}^b$		0.63	1.67	2.38	3.44
	$DCG ext{-}FS ext{-}CCSD^c$		0.62	1.61	2.32	3.47
	Exp^d		0.64	1.40	2.23	3.35

^aRef. [47].

reference in the interaction space should be viewed with caution. The results are quite sensitive to the nature of the reference as well as the number of scalar states included in the interaction space.

5. Conclusion

A cost-effective composite approach, called sf-X2C-S-TD-DFT-SOC, has been proposed for fine-structure calculations of both closed-shell and open-shell systems. The essential merit of the approach lies in that the scalar-excited states are properly spin adapted subject to infinite order scalar relativity, whereas their spin-orbit splittings are accounted for by a first-order molecular mean-field operator. Pilot applications reveal that this approach is fairly accurate and can hence be recommended as an alternative to the genuine 4C/2C-TD-DFT, whose moment adaptation is technically rather difficult, if not impossible.

Among others, two further developments of sf-X2C-S-TD-DFT-SOC should be made. First, the treatment of scalar-excited states of spin $S_f = S_i - 1 > 0$ requires reconsiderations. According to the preliminary experimentations, such states cannot somehow be obtained accurately by the current X-TD-DFT. This is again due to problems associated with the approximate XC kernel. The RPA corrections should be refined for this particular case. Once this is solved, the inclusion of such states in the SOC matrix will permit the

evaluation of, e.g., zero-field splittings of high-spin multiplets. Second, it might be better to take scalar-excited states from different references as the basis for spin—orbit interactions. Compared with the common set of orbitals, the use of different orbitals for different configurations introduces naturally orbital relaxations on the one hand, and can handle certain double excitations on the other. The required matrix elements between non-orthogonal determinants can be simplified by, e.g., the bi-orthogonal transformation technique. Works along these directions are being undertaken in our laboratory.

Acknowledgements

The research of this work was supported by grants from the National Natural Science Foundation of China (Project Nos. 21033001, 21273011, 21290190 and 21173006).

References

- [1] E. Runge and E.K.U. Gross, Phys. Rev. Lett. 52, 997 (1984).
- [2] M.E. Casida, J. Chem. Phys. 122, 054111 (2005).
- [3] Z. Li and W. Liu, J. Chem. Phys. 135, 194106 (2011); (E) 138, 029904 (2013). However, the actual implementation and, therefore, the results were all correct.
- [4] D. Jacquemin, V. Wathelet, E.A. Perpète, and C. Adamo, J. Chem. Theory Comput. 5, 2420 (2009).
- [5] Z. Li and W. Liu, J. Chem. Phys. 133, 064106 (2010).
- [6] Z. Li, W. Liu, Y. Zhang, and B. Suo, J. Chem. Phys. 134, 134101 (2011).

^bRef. [52]

^cRef. [52]. The Gaunt contribution was estimated at the mean-field level.

^dRef. [54].

- [7] F. Wang and W. Liu, J. Chin. Chem. Soc. (Taipei) 50, 597 (2003).
- [8] J. Gao, W. Liu, B. Song, and C. Liu, J. Chem. Phys. 121, 6658 (2004).
- [9] J. Gao, W. Zou, W. Liu, Y. Xiao, D. Peng, B. Song, and C. Liu, J. Chem. Phys. 123, 054102 (2005).
- [10] D. Peng, W. Zou, and W. Liu, J. Chem. Phys. 123, 144101 (2005).
- [11] M.E. Casida, in *Recent Advances in Density Functional Methods*, edited by D.P. Chang (World Scientific, Singapore, 1995), Vol. 1.
- [12] D. Peng, J. Ma, and W. Liu, Int. J. Quantum Chem. 109, 2149 (2009).
- [13] R. Bast, H.J. Aa. Jensen, and T. Saue, Int. J. Quantum Chem. 109, 2091 (2009).
- [14] W. Xu, Y. Zhang, and W. Liu, Sci. China Ser. B 52, 1945 (2009).
- [15] Y. Zhang, W. Xu, Q. Sun, W. Zou, and W. Liu, J. Comput. Chem. 31, 532 (2010).
- [16] F. Wang and T. Ziegler, J. Chem. Phys. 122, 204103 (2005).
- [17] A. Nakata, T. Tsuneda, and K. Hirao, J. Chem. Phys. 135, 224106 (2011).
- [18] D. Sangalli, P. Romaniello, G. Onida, and A. Marini, J. Chem. Phys. 134, 034115 (2011).
- [19] M. Huix-Rotllant, A. Ipatov, A. Rubio, and M.E. Casida, Chem. Phys. 391, 120 (2011).
- [20] P. Elliott, S. Goldson, C. Canahui, and N.T. Maitra, Chem. Phys. 391, 110 (2011).
- [21] E. Fromager, S. Knecht, and H.J. Aa. Jensen, J. Chem. Phys. 138, 084101 (2013).
- [22] F. Wang and T. Ziegler, J. Chem. Phys. 123, 154102 (2005).
- [23] Z. Li, Y. Xiao, and W. Liu, J. Chem. Phys. 137, 154114 (2012).
- [24] Z. Li, Y. Zhang, Y. Xiao, and W. Liu (unpublished)
- [25] W. Liu, Mol. Phys. 108, 1679 (2010).
- [26] Z. Li and W. Liu, J. Chem. Phys. 136, 024107 (2012).
- [27] M. Seth and T. Ziegler, J. Chem. Phys. 123, 144105 (2005).
- [28] B.A. Hess, C.M. Marian, U. Wahlgren, and O. Groppen, Chem. Phys. Lett. 251, 365 (1996).
- [29] J. Tatchen and C.M. Marian, Chem. Phys. Lett. 313, 351 (1999).
- [30] B. Schimmelpfennig, AMFI: An Atomic Mean Field Integral Program (University of Stockholm, Stockholm, Sweden, 1996).
- [31] W. Liu, G. Hong, D. Dai, L. Li, and M. Dolg, Theor. Chem. Acc. 96, 75 (1997).
- [32] W. Liu, F. Wang, and L. Li, J. Theor. Comput. Chem. 2, 257 (2003).

- [33] W. Liu, F. Wang, and L. Li, in *Recent Advances in Relativis-tic Molecular Theory*, Recent Advances in Computational Chemistry, edited by K. Hirao and Y. Ishikawa (World Scientific, Singapore, 2004), Vol. 5, p. 257.
- [34] W. Liu, F. Wang, and L. Li, in Encyclopedia of Computational Chemistry (electronic edition), edited by P. von Ragué Schleyer, N.L. Allinger, T. Clark, J. Gasteiger, P.A. Kollman, H.F. Schaefer III, and P.R. Schreiner (Wiley, Chichester, UK, 2004).
- [35] S.H. Vosko, L. Wilk, and M. Nusair, Can. J. Phys. 58, 1200 (1980).
- [36] A.D. Becke, Phys. Rev. A 38, 3098 (1988).
- [37] C. Lee, W. Yang, and R.G. Parr, Phys. Rev. B 37, 785 (1988).
- [38] A.D. Becke, J. Chem. Phys. 98, 5648 (1993).
- [39] P.J. Stephens, F.J. Devlin, C.F. Chabalowski, and M.J. Frisch, J. Phys. Chem. 98, 11623 (1994).
- [40] T. Yanai, D.P. Tew, and N.C. Handy, Chem. Phys. Lett. 393, 51 (2004).
- [41] F. Wang and T. Ziegler, J. Chem. Phys. 121, 12191 (2004).
- [42] F. Wang and T. Ziegler, J. Chem. Phys. 122, 074109 (2005).
- [43] P.-O. Widmark, P.-Å. Malmqvist, and B.O. Roos, Theor. Chim. Acta 77, 291 (1990).
- [44] B.O. Roos, R. Lindh, P.-Å. Malmqvist, V. Veryazov, and P.-O. Widmark, J. Phys. Chem. A 108, 2851 (2005).
- [45] B.O. Roos, R. Lindh, P.-Å. Malmqvist, V. Veryazov, and P.-O. Widmark, J. Phys. Chem. A 109, 6575 (2005).
- [46] A. Kramida, Yu. Ralchenko, J. Reader, and NIST ASD Team, NIST Atomic Spectra Database (ver. 5.0). (National Institute of Standards and Technology, Gaithersburg, MD, 2012). http://physics.nist.gov/asd.
- [47] Z. Tu, F. Wang, and X. Li, J. Chem. Phys. 136, 174102 (2012).
- [48] D. Yang, F. Wang, and J. Guo, Chem. Phys. Lett. 531, 236 (2012).
- [49] B.O. Roos and P.-Å. Malmqvist, Phys. Chem. Chem. Phys. 6, 2919 (2002).
- [50] J. Dufayard, B. Majournat, and O. Nedelec, Chem. Phys. 128, 537 (1988).
- [51] N.S. Mosyagin, A.V. Titov, E. Eliav, and U. Kaldor, J. Chem. Phys. 115, 2007 (2001).
- [52] L. Visscher, E. Eliav, and U. Kaldor, J. Chem. Phys. 115, 9720 (2001).
- [53] K.P. Huber and G. Herzberg, Molecular Spectra and Molecular Structure IV. Constants of Diatomic Molecules (Van Nostrand Reinhold, New York, 1979).
- [54] M.C.R. Cockett, R.J. Donovan, and K.P. Lawley, J. Chem. Phys. 105, 3347 (1996).